Polymer Bulletin (2024) 81:3459–3478
https://doi.org/10.1007/s00289-023-04879-2

ORIGINAL PAPER

Wound healing potential of sodium alginate-based topical gels loaded with a combination of essential oils, iron oxide nanoparticles and tranexamic acid

X. Nqoro[1] · S. A. Adeyemi[2] · P. Ubanako[2] · D. T. Ndinteh[3] · P. Kumar[2] · Y. E. Choonara[2] · B. A. Aderibigbe[1]

Received: 10 December 2022 / Revised: 5 April 2023 / Accepted: 28 May 2023 /
Published online: 10 June 2023
© The Author(s) 2023

Abstract

Wound management is a key feature in saving people's lives, and regardless of the wound size, using appropriate wound dressing is crucial. Alginate-based topical gels loaded with 2 mL essential oils (eucalyptus, lavender and rosemary oil) in combination with 30 mg magnetite (Fe_3O_4) nanoparticles and 70 mg tranexamic acid were prepared. Carbopol was used as a gelling agent and as a surfactant to disperse the EO. X-ray diffraction (XRD) and scanning electron microscope (SEM) confirmed the successful formation of Fe_3O_4 nanoparticles. The Fourier transform infrared spectroscopy revealed the absence of a chemical interaction between the iron nanoparticles, tranexamic acid, essential oils and the gel matrix. The gel formulations displayed pH, spreadability and viscosity in the range of 6.8–7.2, 5.4–10.1 cm and viscosity (3444–1260 cp) after 120 s, respectively. The in vitro wound healing studies of the wound dressings revealed a wound closure of 99% on day 3. Their antibacterial and blood clotting potential was significant compared to the control. The wound healing capability of these formulations makes them potential wound dressings for treating bleeding and infected wounds.

Keywords Eucalyptus oil · Lavender oil · Rosemary oil · Iron oxide nanoparticles · Tranexamic acid

✉ B. A. Aderibigbe
blessingaderibigbe@gmail.com

[1] Department of Chemistry, University of Fort Hare, Alice Campus, Alice, Eastern Cape, South Africa

[2] Wits Advanced Drug Delivery Platform Research Unit, Department of Pharmacy and Pharmacology, School of Therapeutic Science, Faculty of Health Sciences, University of the Witwatersrand, Johannesburg, South Africa

[3] Department of Applied Chemistry, University of Johannesburg, Doornfontein Campus, Johannesburg, South Africa

Introduction

Wound healing is a complex process comprising various pathways and the involvement of different cell types (*i.e.* keratinocytes, immune, myoblast, endothelial, fibroblast, etc.) that promote the wound healing process. The process of wound healing can be classified based on the type of wound, *i.e.* (acute or chronic wound). Acute wounds heal within a limited time of 1–12 weeks, whereas chronic wounds exceed the predicted period [1]. Several limitations antagonize the wound healing process, such as alcohol, bacterial infection, old age, using inappropriate wound dressings and health conditions (*i.e.* haemophilia, diabetes, obesity, cancer, etc.). These factors not only delay the wound healing process but also result in a wound becoming chronic [2]. Therefore, it is of great importance to take good care of wounds using appropriate wound dressings irrespective of their size to avoid further complications. Over the years, different wound dressings have been developed to accelerate the wound healing process. An ideal wound dressing should be non-toxic, protect against bacterial invasion and the external environment, be biocompatible, retain a moist environment, be biodegradable, stimulate cell proliferation and migration and induce rapid wound healing [3–5]. Biopolymers exhibit interesting properties that make them suitable for developing wound dressings with the aforementioned features of an ideal wound dressing, and among them is sodium alginate (SA), a brown seaweed-derived polysaccharide [6].

Alginate is composed of α- L-guluronic acid (G- blocks) and β-D-mannuronic acid (M- blocks) linked by $1 \rightarrow 4$ glycosidic bonds [7, 8]. Alginate-based dressings have attracted great attention due to their unique features, including good gelling properties, controlled release properties, high haemostatic effects, hydrophilicity and stabilization of dispersions and the capability to induce regeneration of tissue [1, 3]. Moreover, they protect wounds from bacterial invasion and promote an accelerated wound healing process [2]. Additionally, they induce a pro-inflammatory signal and activate macrophages useful in resolving inflammation [9]. Batista et al. reported hybrid alginate/chitosan aerogels with antibacterial activity against *S. aureus* and *K. pneumoniae* that induced a 75% wound scratch reduction in 48 h post-injury [10]. Raguvaran et al. formulated sodium alginate/gum acacia hydrogels encapsulated with ZnO to inhibit the bacterial growth of *P. aerigunosa* and *B. cereus* [4]. Alginate biomaterials are good carriers of antibiotics, metal nanoparticles, bioactive agents, etc. [11].

The use of metal-based nanoparticles due to their outstanding features such as optical, catalytic, magnetic, bio-separation of DNA and proteins and antibacterial properties has enabled their use in various biomedical applications. Iron oxide nanoparticles (Fe_nO_n) occur in different forms as hematite (α-Fe_2O_3), maghemite (g-Fe_2O_3) and magnetite (Fe_3O_4) [12]. The most commonly used iron oxides in wound management are maghemite (g-Fe_2O_3) and magnetite (Fe_3O_4); however, there is not enough information on their wound healing mechanism. Shabanova et al. reported thrombin@ Fe_3O_4NPs for the management of internal bleeding; these NPs displayed non-toxic effects against HeLa and HELF cells,

and they rapidly promoted local haemostasis effect [13]. Bioactive agents such as tranexamic acid, a synthetic compound derived from amino acid lysine, are responsible for the inhibition of fibrinolysis by hindering plasminogen activation, and thus, reducing plasmin formation and preventing fibrin network destruction that leads to stable blood clot formation [14–17]. Bhattacharya et al. reported tranexamic acid-loaded gellan gum-based polymeric beads with a prolonged cumulative release of over 90% of tranexamic acid at pH 7.4 [18].

The loading of essential oils (EO) in biopolymer-based dressing has also drawn a lot of attention in wound management. Mahmood et al. reported gellan gum-based hydrogel films loaded with lavender or tea tree EO with ofloxacin with significant antibacterial activity against *E. coli* and *S. aureus.* The films also promoted a 98% wound reduction within 10 days [19]. *lavandula aspic L.* (lavender EO)-based ointment prepared by Djemaa et al. revealed a 98% wound reduction after 14 days post-injury [20]. Khezri et al. prepared polymer-based nanostructured lipids carriers (NLC) loaded with rosemary oil. The lipids promoted complete wound healing within 12 days [21]. The prepared NLCs induced collagen production, re-epithelialization, fibroblast infiltration, increased vascularization and displayed antibacterial activity against *S. epidermidis, E. coli, L. monocytogenes, P. aeruginosa* and *S. aureus*. Liakos et al. reported SA-based films loaded with a variety of EO (lavender, eucalyptus, elicriso italic, lemongrass, cinnamon, peppermint, tea tree, chamomile blue and lemon). The films exhibited promising wound healing and antimicrobial effects against *C. albicans* and *E. coli* [22].

It is important to select an ideal wound dressing for the management of bleeding and infected wounds. Based on the good reports of the wound healing effects of essential oils, we developed SA/EO-based topical gels composed of sodium alginate, carbopol and different essential oils (*i.e*. rosemary, lavender and eucalyptus oil). These topical formulations were also loaded with iron oxide (Fe_3O_4) nanoparticles and tranexamic acid. The formulations were characterized using FTIR, pH, viscosity and spreadability, followed by in vitro cytotoxicity, blood clotting assay, antibacterial evaluation and wound healing studies.

Materials

Solvents and reagents

Distilled water was used to prepare the topical gels. The materials (sodium alginate, carbopol 940, methylparaben, propylene glycol, triethylamine, potassium hydroxide, ethylene glycol and tranexamic acid (TA)) were of ≥ 95% purity and purchased from Merck Chemicals, South Africa. The essential oils (EO), eucalyptus oil (Euc), lavender oil (Lav) and rosemary (Rose) with a 98–99.9% purity were purchased from Clicks Pharmacy, South Africa. The materials were all used without further purification.

Experimental

Fe_3O_4 nanoparticles preparation

Iron oxide nanoparticles were prepared based on the method reported by Fatima et al. [23]. $FeSO_4{\cdot}7H_2O$ (0.2780 g) was dissolved in 5 mL ethylene glycol to form a homogenous solution. KOH (0.5 M) was dissolved in 8 mL, and then, this solution was added dropwise to the solution of $FeSO_4{\cdot}7H_2O$ (0.2780 g) in ethylene glycol with constant stirring. The resultant solution was then stirred at 200 °C for 24 h, and black solids was formed. The black solids were separated using a magnet separation method, washed with ethanol/water and dried at 40 °C for 6 h.

Preparation of topical gels

The topical gel formulations were prepared according to Table 1. A ratio of 1:1 sodium alginate to carbopol was used to prepare the topical gels in 10 mL distilled water, with continuous stirring at 200–600 rpm until a clear gel was formed. The essential oil was added with continuous stirring at room temperature, resulting in the formation of a gel emulsion. Carbopol was used as a gelling agent and a surfactant/emulsifier to disperse the essential oil. Methylparaben was also added and used as a preservative. TA and iron oxide were added to the prepared gel emulsions with continued stirring for 20 min. Triethylamine was used to adjust the pH of the prepared gels, and propylene glycol was used as a penetration enhancer. The prepared gel formulations were stored in the refrigerator for further analysis.

Table 1 The composition of the topical gel formulations

Code	Polymers		NPs		EO		Drug	Distilled water (mL)
	SA	Carbopol	Fe_3O_4	Euc	Lav	Rose	TA	
SA-Blank	100 mg	100 mg	–	–	2 mL	–	–	10
SA/Lav	100 mg	100 mg	–	–	–	2 mL	–	10
SA/Rose	100 mg	100 mg	–	2 mL	–	–	–	10
SA/Euc	100 mg	100 mg	–	–	2 mL	–	30 mg	10
SA/Lav/ Fe_3O_4	100 mg	100 mg	–	–	–	2 mL	30 mg	10
SA/Rose/ Fe_3O_4	100 mg	100 mg	–	2 mL	–	–	30 mg	10
SA/Euc/ Fe_3O_4	100 mg	100 mg	70 mg	–	–	2 mL	30 mg	10
SAT/Euc/ Fe_3O_4	100 mg	100 mg	70 mg	–	2 mL	–	30 mg	10
SAT/Rose/ Fe_3O_4	100 mg	100 mg	70 mg	2 mL	–	–	30 mg	10
SAT/Lav/ Fe_3O_4	100 mg	100 mg	–	–	2 mL	–	–	10

Characterization

Attenuated total reflection Fourier transform infrared spectroscopy (ATR-FTIR)

Attenuated total reflection Fourier transform infrared spectroscopy (ATR-FTIR) was performed on the gel formulations using Spectrum Two PerkinElmer. Their spectra were recorded within the range of 4000–500 cm^{-1} using Origin software.

Spreadability

Spreadability is used to determine the rate at which the gels spread on the wound surface. 0.1 g of the gel with an initial diameter in the range of 1–1.3 cm was placed on a glass slide, and a second glass slide was carefully placed on top of the slide containing the gel. A 100 g mass was placed on top of the two glass slides for 10 min, and the spreadability was determined in cm [24–28].

Viscosity

Brookfield viscometer (DV-1) was used to determine the viscosity (cP) of the prepared gel formulations. Spindle 63 (LV3) was rotated at a speed of 50 and 100 rpm. The reading was recorded at 1- and 2-min time intervals and at a temperature of 37 °C.

pH evaluation

The pH of the gel formulations was evaluated using a digital pH metre.

Scanning electron microscope (SEM)

The SEM was used to evaluate the surface morphology and elemental composition of the prepared nanoparticles. It was performed on a JEOL (JSM- 6390 LV) scanning electron microscope, Japan, at an accelerating voltage of 15 kV [29].

X-ray diffraction (XRD)

XRD thermographs were reported on a Bruker D8 Discover equipped with a proportional counter using Cu-Kα radiation. Data were collected within the range of $2\Theta = 5–60°$, scanning at 1.5° min^{-1} with a time constant filter of 0.38 s per step and 6.0 mm slit width. Samples were mounted on a slide with a silicon wafer. The X-ray diffraction data were handled using the Profex program (evaluation curve fitting). Baseline correction was achieved by the elimination of a spline feature

adapted to the curved base on each diffraction pattern. It was used to study the crystalline nature of magnetite nanoparticles.

In Vitro antibacterial analysis

The antibacterial evaluation was performed to determine the antibacterial activity of the wound dressings against selected strains of bacteria. Three controls were used, ampicillin (AMP), streptomycin (STM) and nalidixic acid (NLD) (Table 2). The minimum inhibitory concentration (MIC) of the formulations was evaluated according to the procedure by Fonkui et al. [30]. The stock solutions were prepared by dissolving 4 mg of each gel formulation in 5 mL of a mixture of DMSO and dH_2O (4:1, v/v). These solutions were then serially diluted (6 times) in 100 µL of nutrient broth in 96 well plates to the desired concentrations (400, 200, 100, 50, 25 and 12.5 µg/mL). 100 µL of each of these solutions was then placed in duplicate and seeded with 100 µL of an overnight bacterial culture. Streptomycin, ampicillin and nalidixic acid were used as positive controls. The negative control contained 50% nutrient broth in DMSO.

In vitro *w*hole blood clot assay

The in vitro haemostasis analysis was performed according to the procedure described by Catanzano et al. on the gel formulations, SA/Rose, SA/Lav, SA/Lav/Fe_3O_4, SAT/Euc/Fe_3O_4, SAT/Rose/Fe_3O_4 and SAT/Lav/Fe_3O_4 at a wavelength of 540 nm [31]. A two-tailed *t*-test using GraphPad was used to evaluate the significant difference between the formulations and the control. The wound dressing, 2 mg was immersed in 200 µL of the whole blood and placed in 15-mL tubes. Blood coagulation on the formulations was activated by adding 20 µL of $CaCl_2$. The wound dressings were then further incubated in a thermostatic incubator for 10 min at 37 °C with gentle shaking. Deionized water (6 mL) was used to

Table 2 Selected bacterial strains used and abbreviations

Bacterial strains	Code
Bacillus subtilis (ATCC19659)	BS
Enterococcus faecalis (ATCC13047)	EF
Escherichia coli (ATCC25922)	EC
Enterobacter cloacae (ATCC13047)	ECL
Mycobacterium smegmatis (MC2155)	MS
Staphylococcus epidermidis (ATCC14990)	SE
Klebsiella oxytoca (ATCC8724)	KO
Klebsiella pneumonia (ATCC13882)	KP
Proteus vulgaris (ATCC6380)	PV
Pseudomonas aeruginosa (ATCC27853)	PA
Proteus mirabilis (ATCC7002)	PM
Staphylococcus aureus (ATCC25923)	SA

haemolyse the red blood cells (RBCs) trapped in the clot. A spectrophotometer was used to measure the relative absorbance (A) of the blood samples diluted to 25 mL at a wavelength of 540 nm [31].

Cytotoxicity evaluation

The in vitro cytotoxicity of the wound dressings was performed to evaluate their biocompatibility using a (3-(4,5-dimethylthiazol-2-yl)-2,5-diphenyltetrazolium bromide)(MTT) assay. The gels SA-Blank, SA/Lav/Fe_3O_4, SAT/Euc/Fe_3O_4, SAT/Rose/Fe_3O_4 and SAT/Lav/Fe_3O_4 were screened against HaCaT cells (immortalized human keratinocytes) which were seeded at a density of 5×10^4 cells/ml in 96-well plates at a volume of 90 µL/well. The experiments were performed in triplicate, and the cytotoxicity results of these gels were analysed by calculating the percentage cell viability using Eq. 1 [32]:

$$\% \text{ Cell viability} = \frac{(\text{ODs} - \text{ODc})}{(\text{ODu} - \text{ODc})} \times 100 \tag{1}$$

where OD_S is the absorbance of the test compound, OD_c is the absorbance of the control, and OD_u is the absorbance of the untreated compound.

Wound healing assay

In vitro wound healing assay was performed based on a procedure adapted from Felice et al., Suarez-Arnedo et al., Cheng et al. and Ranzato et al. [33–36]. It was only performed on SAT/Lav/Fe_3O_4 formulation to evaluate its wound healing ability within 3 days. The cell migration was quantified using ImageJ image processing software. The wound closure was calculated using the following Eq. 2 [37]:

$$\% \text{ Wound closure} = \frac{\text{wound area day 0} - \text{wound closure day 72}}{\text{wound closure day 0}} \times 100 \tag{2}$$

Statistical analysis

Cytotoxicity and wound healing experiments were performed in triplicates. An unpaired Student's *t*-test was performed using GraphPad to study the statistical significance of the treated versus untreated samples, and $p \leq 0.05$ was considered statistically significant.

Results and discussion

FTIR

The ATR-FTIR spectra of the prepared gels are depicted in Fig. 1a–c. The pure lavender oil exhibited an absorption peak at 3468 cm^{-1}, resulting from O–H stretch due to the presence of terpene-4-ol and linalool [38]. The intense peak at 2946 cm^{-1} is attributed to the aliphatic C–H stretch. The strong peak at 1740 cm^{-1} is attributed to the C=O carbonyl group, indicating the presence of the major components of lavender oil, such as lavandula acetate, linalool, camphor and linalyl acetate [39, 40]. The C–O stretch bend visible at 1253 cm^{-1} further confirms the presence of an ester component of the lavender oil [38, 39]. The peaks at 917, 1018 and 1253 cm^{-1} correspond to the C–H deformations [39, 40]. SA/Lav/Fe_3O_4 and SAT/Lav/Fe_3O_4 displayed broad characteristic peaks at 3460 cm^{-1} corresponding to the O–H stretching [24]. The vibration bend at 2923 cm^{-1} is attributed to C–H stretch present in both polymer and lavender oil components. The twin peaks at 1641 and 1732 cm^{-1} are due to the C=O stretching carbonyl group [38]. There was no major difference in the absorption peaks found in the formulations, SA/Lav, SA/Lav/Fe_3O_4 and SAT/Lav/Fe_3O_4. The characteristic peaks of lavender oil were retained in all the formulations,

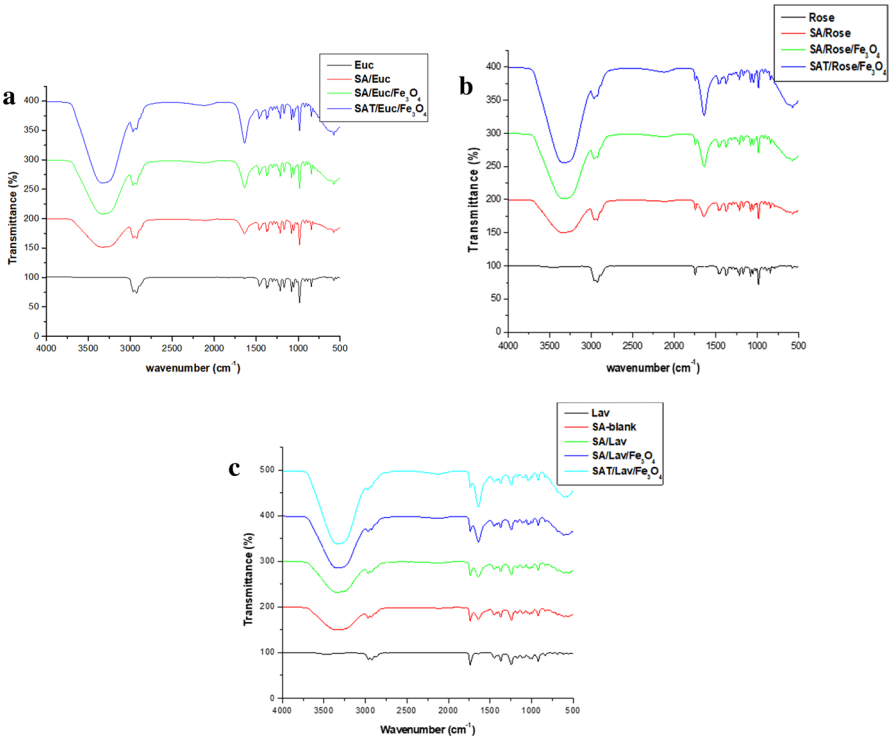

Fig. 1 FTIR spectra **a** SA/Euc, **b** SA/Rose and **c** SA/Lav-based formulations

SA/Lav, SA/Lav/Fe_3O_4 and SAT/Lav/Fe_3O_4. The FTIR spectra of eucalyptus oil showed vibration bend at 2948 cm^{-1} attributed to asymmetrical and symmetrical bending of C–H stretching [41]. The vibration bends at 968, 1079–1203 and 1354 cm^{-1}, corresponding to the symmetrical bending of the CH_2 plane, C–O–C stretching and C–O–H deformation, indicating the presence of 1,8-cineol and citronella, active components of eucalyptus oil.

In the FTIR spectra of the formulations containing lavender oil, SA/Euc, SA/Euc/Fe_3O_4 and SAT/Euc/Fe_3O_4, there was no major difference. The presence of eucalyptus oil components was retained in all the formulations with major characteristic peaks visible at 968, 1079–1203, 1354 and 2948 cm^{-1} relating to CH_2 plane, asymmetric C–O–C stretching, C–O–H deformation and C–H symmetric bending, respectively. Additionally, a broad vibrational bend was observed at 3457 cm^{-1} due to O–H bending in alginate [42]. The FTIR spectrum of rosemary oil revealed vibration bending for C–H methylene group and O–H at 2932 cm^{-1} and 3486 cm^{-1}, respectively [43, 44]. The characteristic peak at 1723 cm^{-1} is attributed to the C=O carbonyl group [44]. The vibration bends at 833, 984, 1085, 1236 and 1330 cm^{-1} indicate the monoterpenes, such as 1,8-cineole present in rosemary oil [45, 46]. The FTIR spectra of SA/Rose/, SA/Rose/Fe_3O_4 and SAT/Rose/Fe_3O_4 revealed similar absorption bends and a broad O–H peak at 3443 cm^{-1}. These formulations showed the presence of rosemary oil which was stable in the polymeric matrix and did not interact with the polymer matrix. The major vibration bends for monoterpenes were retained [47]. The FTIR spectra of the gel formulations revealed the successful loading of the essential oils.

Spreadability

The successful preparation of the gel formulations was confirmed by FTIR analysis. The gels were then further evaluated for their spreadability, pH, stability and viscosity. The pH of the gels was in the range of 6.8–7.2 which is compatible with skin application. The prepared topical gels exhibited spreadability within the range of 5.4–10.1 cm (Table 3). SA/Rose exhibited lower spreadability values compared to the formulations loaded with either iron oxide alone or a combination of iron oxide and tranexamic acid. The SA/Lav formulation revealed a decreased spreadability behaviour. SA/Euc topical gels showed no significant spreadability trend. The contact time of the topical that aids the healing efficiency of topical gels is influenced by their spreadability [26]. The viscosity of the prepared formulations was recorded at 50 rpm (revolution per minute) in 30 and 120 s. The viscosity of all topical gel formulations was significantly lower compared to the pure gel (SA-Blank). SA-Blank, SA/Rose/Fe_3O_4 and SAT/Rose/Fe_3O_4 revealed a shear-thinning behaviour as time increased from 30 to 120 s when compared to other formulations. After 12 months of storage in a refrigerator, all the prepared formulation maintained their physical and chemical state, showing their stability under long-term storage.

Table 3 Spreadability, pH and stability results of the prepared topical gels

Sample ID	Spreadability	pH	Viscosity 50 rpm	
			30 s	120 s
SA-Blank	1.3–10.1 cm	6.8	5424 cp	5381 cp
SA/Lav	1.7–9.1 cm	6.9	3396 cp	3444 cp
SA/Rose	1.3–7.3 cm	6.8	2232 cp	2244 cp
SA/Euc	1.5–6.8 cm	7.1	2829 cp	2841cp
SA/Lav/Fe_3O_4	1.3–5.4 cm	6.8	3288 cp	3300 cp
SA/Rose/Fe_3O_4	1.5–8.3 cm	7.2	1284 cp	1260 cp
SA/Euc/Fe_3O_4	1.5–6.5 cm	7.0	2892 cp	2928 cp
SAT/Euc/Fe_3O_4	1.4–7.5 cm	7.1	3060 cp	3108 cp
SAT/Rose/Fe_3O_4	1.5–10 cm	6.9	1743 cP	1716 cP
SAT/Lav/Fe_3O_4	1.5–6.2 cm	7.0	2232 cP	2280 cP

SEM, UV–vis and XRD

The SEM images of the prepared Fe_3O_4 nanoparticles (Fig. 2a, b) revealed aggregated and a cluster of spherical-shaped morphology. Pirsa et al. reported similar morphology, and the particle aggregation is influenced by an increase in the particle's surface energy and decreased particle size [48]. Similar findings were also reported by Kulkarni et al., Hariani et al. and Awwad et al. [49–51]. The UV–vis of Fe_3O_4 nanoparticles revealed absorbance at 299 nm, confirming the successful preparation of the nanoparticles (Supp Fig. 1). The XRD graph displayed prominent crystalline characteristic 2Θ peaks at 21.7°, 30.01°, 31.01°, 36°, 43.6° and 52.4° that were assigned to the crystal planes of (111), (220), (311), (222), (400) and (422) inverse cubic spinel magnetite, respectively, for Fe_3O_4 nanoparticles (Supp Fig. 2). A similar finding was reported by Qureshi et al. for hematite and magnetite nanoparticles [52]. The peaks confirmed the crystalline nature of the prepared Fe_3O_4 nanoparticles [48]. The SEM images, UV spectra and XRD characteristic peaks confirmed the successful synthesis of Fe_3O_4 nanoparticles.

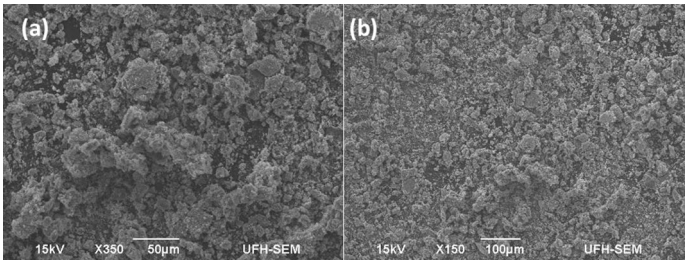

Fig. 2 SEM images of iron oxide nanoparticles at different magnifications

Table 4 Antimicrobial activity of the prepared SA gels against different strains of bacteria

Minimum inhibitory concentration (MIC, μg/mL)												
Sample ID	Gram-positive					Gram-negative						
	BS	EF	SE	SA	MS	ECL	PV	KO	PA	PM	EC	KP
SA-Blank	–	–	–	200	–	–	50	–	12.5	–	–	200
SA/Lav	–	–	–	200	–	–	12.5	–	12.5	–	100	200
SA/Rose	15.625	15.625	–	31.5	–	15.625	–	15.625	15.625	15.625	–	–
SA/Euc	–	–	–	200	–	–	12.5	–	12.5	–	12.5	200
SA/Lav/Fe_3O_4	15.625	15.625	15.625	62.5	–	15.625	15.625	15.625	15.625	15.625	–	–
SA/Rose/Fe_3O_4	15.625	15.625	–	31.5	–	15.625	–	15.625	15.625	15.625	–	–
SA/Euc/Fe_3O_4	–	–	–	200	–	–	12.5	–	12.5	–	100	200
SAT/Euc/Fe_3O_4	–	–	–	200	–	–	12.5	–	12.5	100	100	100
SAT/Rose/Fe_3O_4	–	–	–	200	–	–	25	–	12.5	–	–	200
SAT/Lav/Fe_3O_4	–	15.625	15.625	62.5	–	15.625	15.625	15.625	15.625	15.625	–	–
TA	–	–	–	200	–	–	12.5	–	12.5	–	–	200
Rose–EO	15.625	15.625	15.625	62.5	–	15.625	–	15.625	15.625	15.625	–	–
Euc–EO	15.625	15.625	–	62.5	–	15.625	–	15.625	15.625	15.625	–	–
Lav–EO	15.625	15.625	–	62.5	–	15.625	–	15.625	15.625	15.625	–	–
Fe_3O_4	25	25	–	–	–	–	12.5	–	12.5	100	100	100
AMP	26	26	26	26	26	26	416	26	64	26	26	26
STM	16	128	8	256	4	512	128	16	128	128	64	512
NLD	16	>512	64	64	512	16	128	8	128	32	512	256

In vitro antibacterial assay

The antibacterial activity (MIC values) of the topical gel formulations is shown in Table 4. The antibacterial activity of the formulations was compared to the controls, AMP, STM and NLD. SA-Blank revealed antibacterial activity mostly against gram-negative strains of bacteria (*P. vulgaris*, *P. aeruginosa*, *K. pneumonia* and *S. aureus*) which is attributed to alginate. Euc-EO exhibited antibacterial activity against *B. subtilis*, *E. faecalis*, *S. aureus*, *E. cloacae*, *K. oxytoca*, *P. aeruginosa* and *P. mirabilis*. SAT/Euc/ Fe_3O_4 showed microbial inhibition against *P. mirabilis*, a species under the same genus as *P. vulgaris*. The microbial inhibition effect displayed by these gel formulations against *S. aureus, E. coli* and *P. aeruginosa;* the commonly resistant strains of bacteria that cause sepsis and other diseases are also found in infected and chronic wounds [53–55]; *P. vulgaris* is reported to be responsible for biofilm and antibiotic resistance [56]. These formulations were effective against gram-negative strains which are considered the most resistant and harmful strains of bacteria [57].

Lav-EO exhibited a microbial inhibition effect similar to Euc-EO. SA/Lav against *S. aureus*, *P. vulgaris*, *P. aeruginosa*, *E. coli* and *K. pneumonia*. The loading of iron oxide nanoparticles in this gel formulation led to a broad spectrum of microbial activity against (*B. subtilis*, *E. faecalis*, *S. epidermidis*, *S. aureus*, *E. cloacae*, *P. vulgaris*, *K. oxytoca*, *P. aeruginosa* and *P. mirabilis*) visible in SA/Lav/Fe_3O_4. Similar results were reported by Mahmood et al. for hydrogel films containing Lav-EO which were more effective against *S. aureus* than *E. coli* [19]. SAT/Lav/Fe_3O_4 exhibited antimicrobial activity similar to SA/Lav/Fe_3O_4 except that it did not inhibit *B. subtilis*. As a spore-forming bacteria, *B. subtilis* is known to possess a much thicker proteinous cell wall which hinders the permeability of nanoparticles [58].

The antibacterial activity of Rose-EO was significant against *B. subtilis*, *E. faecalis*, *S. epidermidis*, *S. aureus*, *E. cloacae*, *K. oxytoca*, *P. aeruginosa* and *P. mirabilis* strains of bacteria. Gel formulations, SA/Rose and SA/Rose/Fe_3O_4 inhibited the same bacteria strains and displayed similar MIC values. The identical antibacterial activity displayed by SA/Rose and SA/Rose/Fe_3O_4 suggests that the encapsulation of iron oxide nanoparticles played no significant role in their antibacterial activity. SAT/Rose/Fe_3O_4 displayed significant antibacterial activity against *S. aureus*, *P. vulgaris*, *P. aeruginosa* and *K. pneumonia*, suggesting that the loading of two or more bioactive agents into the gels composed of SA/Rose decreased their antibacterial activity. Khezri et al. reported polymer-based nanostructured lipid carriers loaded with rosemary oil to inhibit the growth of *P. aeruginosa* and *S. aureus* [21]. The antimicrobial activity of the formulations reveals that they are promising therapeutics for treating infected wounds.

In vitro whole blood clot assay

Apart from wound dressings exhibiting promising antibacterial activity, haemostatic activity is a crucial feature needed in wound dressings used in treating bleeding wounds. Haemostatic material should be able to form clots and thus stop bleeding

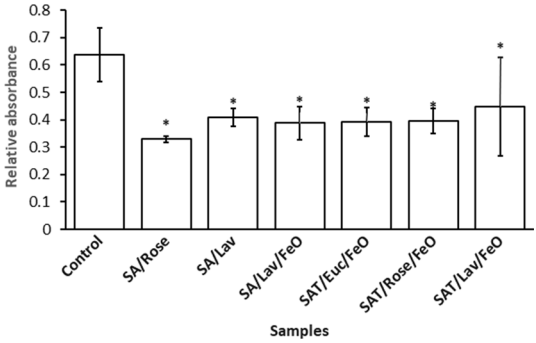

Fig. 3 Whole blood clot analysis (Error bars ± std * "*p*-value < 0.05")

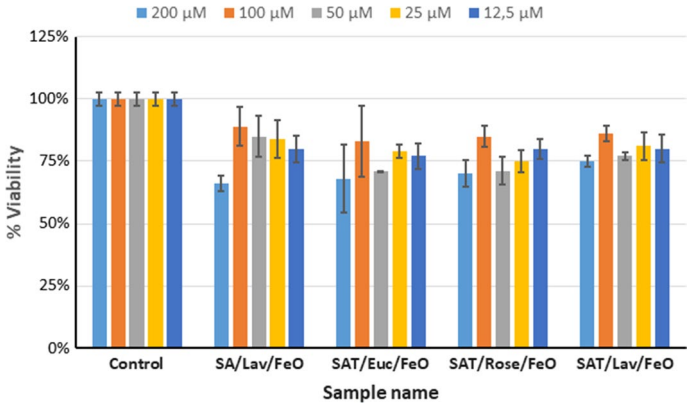

Fig. 4 In vitro % cell viability of the control and selected SA/EO-based topical gels (Error bars ± std)

within a limited amount of time to hinder excessive bleeding. Absorbance values of all the prepared topical gels were lower compared to the control with (*p*-values = 0.0051, 0.0255, 0.0177, 0.0188, 0.0196 and 0.0371 for SA/Rose, SA/Lav, SA/Lav/Fe_3O_4, SAT/Euc/Fe_3O_4, SAT/Rose/Fe_3O_4 and SAT/Lav/Fe_3O_4, respectively. These results suggest that the prepared gels can form prevent excessive bleeding, as stated by Huang et al. that lower absorbance values are equivalent to larger blood clot size [59]. SA/Rose exhibited the lowest absorbance values compared to all other formulations with (*p*-value > 0.05) except for SA/Lav (*p*-value = 0.0156). Among the formulations, there was no significant difference in terms of the *p*-value. Iron oxide nanoparticles and tranexamic acid played no significant role when loaded on the prepared SA/EO gels, and similar blood clotting behaviour was observed across all the gels used in this study. However, rose oil formulations revealed promising blood clotting potential compared to lavender oil formulations (*p*-value < 0.05). SA/EO gels displayed good potential in faster clot formation and this compliments their antibacterial efficiency results, suggesting that they are potential wound dressings for treating bleeding and infected wounds. The biocompatible nature of wound dressing is also important when designing a wound dressing (Figs. 3 and 4).

In vitro cytotoxicity

A wound dressing must have low toxicity because it will be in direct contact with the affected area, to avoid further complications. The in vitro cytotoxicity assay was investigated using HaCaT cells, and the formulation was tested at different concentrations. In relation to the antibacterial activity and blood clotting results, the essential oil-loaded gels revealed promising wound healing activity and showed no signs of toxicity even at a higher concentration of 200 µM. The loading of the essential oils and nanoparticles significantly improved the viability of these scaffolds (p-value < 0.05) at both 100 and 12.5 µM compared to the SA-Blank gel formulation. However, there was no significant difference between the blank and SAT/Rose/Fe_3O_4 at a concentration of 50 µM (p-value 0.0984). The prepared SA/EO-based gels displayed the highest cell viability at 100 µM and showed no significant difference compared to the control except for SAT/Rose/Fe_3O_4 (p-value = 0.0037) and SAT/Lav/Fe_3O_4 (p-value = 0.0024). According to the International Standard ISO10993-12:2009, a compound whose treatment results in a cell viability percentage of less than 70% is considered cytotoxic [60]. The SA/EO-based topical gels reported in this study revealed a non-cytotoxic effect against HaCaT cells, revealing their safe use as topical wound dressings. SAT/Lav/Fe_3O_4 exhibited a 75% cell viability across all the concentrations tested and was selected for in vitro wound healing.

In vitro wound healing assay

SAT/Lav/Fe_3O_4 exhibited outstanding antibacterial activity, high cell viability and rapid blood clotting potential, and its wound healing potential was investigated in vitro and compared to the untreated cells from 0 to 72 h (Table 5). Cell proliferation and migration are essential phases of the wound healing process [61]. Cell migration was evaluated using an inverted light microscope, and the micrographs are reported in Fig. 5a, b for treated and untreated groups. The untreated group displayed a slower rate of wound reduction (24%) in 72 h post-injury when compared to the SAT/Lav/Fe_3O_4 gel formulation that induced a higher rate of HaCaT cell migration and proliferation with 99% wound closure. These findings suggest that SAT/Lav/Fe_3O_4 promoted high cell migration to the affected area. The rapid wound closure presented by this formulation is influenced by the synergistic effect resulting from the combination of lavender oil, tranexamic acid and Fe_3O_4 nanoparticles.

Table 5 The wound healing effect of SAT/Lav/Fe_3O_4 compared to that of untreated (mean ± STD, $n = 3$)

Time (h)	Area (mm^2)	
	Untreated	SAT/Lav/Fe_3O_4
0	832.97	534.85
24	707.84 ± 12.96	285.60 ± 31.92
48	669.77 ± 25.01	117.82 ± 12.93
72	636.11 ± 68.78	4.31 ± 1.49
Total reduction	196.86 = 24%	530.55 = 99%

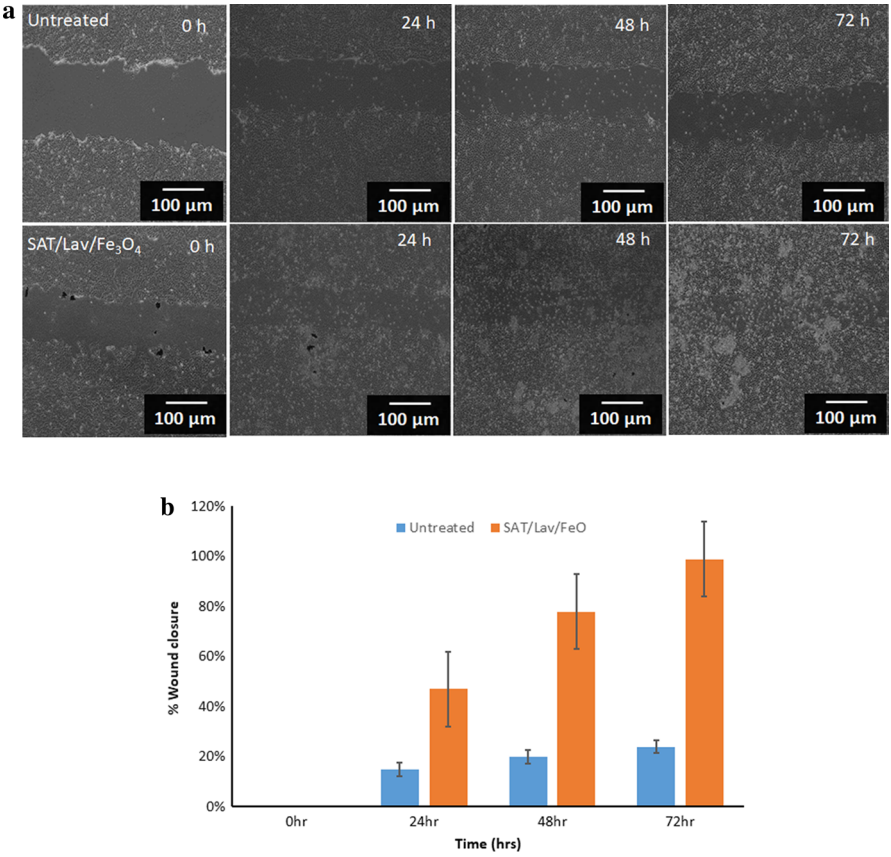

Fig. 5 **a** Micrographs showing migration of cells for untreated and SAT/Lav/Fe_3O_4 from 0 to 72 h, **b** a graph showing the percentage of wound closure in vitro over 72 h post-treatment

The spreadability and viscosity of this formulation also influenced its wound healing potential [26]. Elmowafy et al. stated that the viscosity of the topical formulations prolongs their contact time at the site of application and the rate of drug delivery [62]. Djemaa et al. developed a Lav-EO-based ointment that induced a 98% wound contraction in 14 days post-injury, revealing the efficacy of lavender oil in wound healing [20]. Lavender oil enhances wound healing by inhibiting lipid peroxidation [20]. It also accelerates wound closure by a rapid reduction in granulation tissue induced by platelet-derived growth factors, promotes granulation tissue formation in the early phase of wound healing and induces collagen replacement from type III to type I, an essential process for tissue remodelling and accelerated wound healing. It also induced the expression of TGF-β, a key molecule that is essential to induce angiogenesis, the proliferation of fibroblasts and matrix production by fibroblasts [63]. TGF-β is also prominent in the rapid formation of granulation tissue and increased production of collagen by fibroblasts, secretion of MMP-13, a collagenase-3 which is essential for the degradation of type III collagen for a replacement

of type I collagen [63, 64]. Lavender oil induces the differentiation of fibroblasts to myofibroblasts in the early phase of wound healing, a process that is stimulated by TGF-β and useful for wound contraction [63, 65].

Similarly, Kozics et al. reported the high antibacterial activity of lavender oil. At a higher concentration of 0.0469% (*w*/*v*), lavender oil did not induce a toxic effect on HaCaT cells in vitro [66]. Prashar et al. reported the non-toxic effect of lavender oil which was dose-dependent. A concentration of 0.125% (*v*/*v*) showed 80–100% cell viability and a concentration of 0.25% (*v*/*v*) revealed a toxic effect on human skin cells in vitro [67]. Moreover, Miastkowska et al. revealed that the cytotoxic effect of lavender oil on HaCaT cells in vitro is influenced by its concentration. A concentration of 0.025% (*v*/*v*) of lavender oil induced a 100% cell viability and 0.390% (*v*/*v*) of lavender oil displayed less than 25% HaCaT cell viability [68]. Kazemi et al. reported nanoemulsions composed of lavender EO and licorice (rhizome and root of *Glycyrrhiza glabra*) extract that accelerated wound contraction by 98% on the 14th day with an increased collagen type I and III expressions, including TGF-β1 [65].

Tranexamic acid is an anti-fibrinolytic drug that is useful in reducing blood loss. However, it also increases collagen synthesis and tensile strength within the granulation tissue, thereby retaining the fibrin matrix. It accelerates normal wound healing by stabilizing the fibrin structures [69]. Fe_3O_4 nanoparticles, on the other hand, induce wound healing by penetrating bacterial biofilm. The combination of Fe_3O_4 nanoparticles with silver nanoparticles revealed a significant penetration of bacterial biofilms [70]. Fe_3O_4 nanoparticles also enhanced the migration of normal adult human dermal fibroblast cells and wound closure [71]. Based on the aforementioned efficacy of Fe_3O_4 nanoparticles, lavender oil and tranexamic acid, combining them in topical gels revealed a synergistic effect. However, more studies are needed to fully understand the mechanisms of action of the formulation in wound healing.

Conclusion

The FTIR spectra of the prepared formulations revealed that the loaded tranexamic acid and iron oxide did not interact with the polymer matrix. The good spreadability and shear-thinning nature of the gels suggest that they will not flow off easily from the site of application. The gels exhibited pH values between 6.7 and 7.2 compatible with skin application. The SEM and XRD results confirmed the successful formation of iron oxide nanoparticles. The MIC values exhibited by SA/EO-based gels showed a broad antibacterial spectrum, even against the common resistant strains of bacteria, *S. aureus* and *E. coli*. SAT/Lav/Fe_3O_4 gel displayed the highest antibacterial efficacy across all the tested strains of bacteria when compared to other gel formulations. The blood clotting potential displayed by these formulations also revealed their capability to promote blood clotting rapidly. The gel formulations loaded with rosemary and eucalyptus oil exhibited lower absorbance values compared to the formulations loaded with lavender oil. Although SAT/Lav/Fe_3O_4 exhibited higher absorbance values when compared to other formulations, it is still an

ideal wound dressing for controlling bleeding and wound healing. The prepared formulations were not toxic to HaCaT cells when tested in vitro and displayed cell viability above 75% at 100 and 12.5 µM. Interestingly, SAT/Lav/Fe_3O_4 displayed high cell migration, revealing its potential to accelerate wound healing. The prepared topical gels are promising dressings for the management of bleeding and microbial-infected wounds. However, further studies entailing biological and in vivo studies of these formulations are still needed.

Supplementary Information The online version contains supplementary material available at https://doi.org/10.1007/s00289-023-04879-2.

Acknowledgements The financial support of Govan Mbeki Research and Development Centre, University of Fort Hare, South Africa Medical Research Council, and National Research Foundation, South Africa towards this research is hereby acknowledged.

Funding Open access funding provided by University of Fort Hare.

Declarations

Conflict of interest The authors hereby declare no conflict of interest.

Open Access This article is licensed under a Creative Commons Attribution 4.0 International License, which permits use, sharing, adaptation, distribution and reproduction in any medium or format, as long as you give appropriate credit to the original author(s) and the source, provide a link to the Creative Commons licence, and indicate if changes were made. The images or other third party material in this article are included in the article's Creative Commons licence, unless indicated otherwise in a credit line to the material. If material is not included in the article's Creative Commons licence and your intended use is not permitted by statutory regulation or exceeds the permitted use, you will need to obtain permission directly from the copyright holder. To view a copy of this licence, visit http://creativecommons.org/licenses/by/4.0/.

References

1. Varaprasad K, Jayaramudu T, Kanikireddy V, Toro C, Sadiku ER (2020) Alginate-based composite materials for wound dressing application: a mini review. Carbohydr Polym 236:116025
2. Riaz A, Sohail M, Usman M, Khaliq T, Kousar M, Khan S, Hussain Z, Munir A (2020) Biological Macromolecules Bioinspired sodium alginate based thermosensitive hydrogel membranes for accelerated wound healing. Int J Biol Macromol 155:751–765
3. Kong F, Fan C, Yang Y, Hoon B, Wei K (2019) 5-hydroxymethylfurfural-embedded poly (vinyl alcohol)/sodium alginate hybrid hydrogels accelerate wound healing. Int J Biol Macromol 138:933–949
4. Raguvaran R, Manuja BK, Chopra M, Thakur R, Anand T, Kalia A, Manuja A (2017) Sodium alginate andgum acacia hydrogels of ZnO nanoparticles show wound healing effect on fibroblast cells. Int J Biol Macromol 96:185–191
5. Bagher Z, Ehterami A, Hossein M, Khastar H (2020) Wound healing with alginate/chitosan hydrogel containing hesperidin in rat model. J Drug Deliv Sci Technol 55:101379
6. Summa M, Russo D, Penna I, Margaroli N, Bayer IS (2018) A biocompatible sodium alginate/povidone iodine film enhances wound healing. Eur J Pharm Biopharm 122:17–24
7. Taemeh MA, Shiravandi A, Korayem MA, Daemi H (2020) Fabrication challenges and trends in biomedical applications of alginate electrospun nano fibers. Carbohydr Polym 228:115419

8. Shalumon KT, Anulekha KH, Nair SV, Nair SV, Chennazhi KP, Jayakumar R (2011) Macromolecules Sodium alginate/poly (vinyl alcohol)/nano ZnO composite nanofibers for antibacterial wound dressings. Int J Biol Macromol 49:247–254
9. Singh B, Varshney L, Francis S (2017) Designing sterile biocompatible moxifloxacin loaded trgacanth-PVA -alginate wound dressing by radiation crosslinking method. Biochem Pharmacol 17:11–17
10. Batista MP, Gonçalves VSS, Gaspar FB, Nogueira ID, Matias AA, Gurikov P (2020) Novel alginate-chitosan aerogel fibres for potential wound healing applications. Int J Biol Macromol 156:773–782
11. Naja M, Osfouri S, Azin R, Zaeri S (2020) Alginate-based electrospun core/shell nanofibers containing dexpanthenol: a good candidate for wound dressing. J Drug Deliv Sci Technol 57:101708
12. Ali A, Zafar H, Zia M, ul Haq I, Phull AR, Ali JS, Hussain A, (2016) Synthesis, characterization, applications, and challenges of iron oxide nanoparticles. Nanotechnol Sci Appl 9:49–67
13. Shabanova EM, Drozdov AS, Fakhardo AF, Dudanov IP, Kovalchuk MS, Vinogradov VV (2018) Thrombin@Fe_3O_4 nanoparticles for use as a hemostatic agent in internal bleeding. Sci Rep 8:1–10
14. Mahmoodzadeh A, Moghaddas J, Jarolmasjed S, Ebrahimi Kalan A, Edalati M, Salehi R (2021) Biodegradable cellulose-based superabsorbent as potent hemostatic agent. Chem Eng J 418:129252
15. Howe N, Cherpelis B (2013) Obtaining rapid and effective hemostasis: Part I update and review of topical hemostatic agents. J Am Acad Dermatol 69:659
16. Austin SK (2021) Haemostasis Med 49:199–204
17. Peng HT (2020) Hemostatic agents for prehospital hemorrhage control: a narrative review. Mil Med Res 7:1–18
18. Bhattacharya SS, Banerjee S, Chowdhury P, Ghosh A, Hegde RR, Mondal R (2013) Tranexamic acid loaded gellan gum-based polymeric microbeads for controlled release: in vitro and in vivo assessment. Colloids Surf B 112:483–491
19. Mahmood H, Khan IU, Asif M, Khan RU, Asghar S, Khalid I, Khalid SH, Irfan M, RehmanF SY, Yousaf AM (2021) In vitro and in vivo evaluation of gellan gum hydrogel films: assessing the co impact of therapeutic oils and ofloxacin on wound healing. Int J Biol Macromol 166:483–495
20. Ben Djemaa FG, Bellassoued K, Zouari S, El Feki A, Ammar E (2016) Antioxidant and wound healing activity of Lavandula aspic L. ointment. J Tissue Viability 25:193–200
21. Khezri K, Farahpour MR, Mounesi Rad S (2019) Accelerated infected wound healing by topical application of encapsulated Rosemary essential oil into nanostructured lipid carriers. Artif Cell Nanomed Biotechnol 47:980–988
22. Liakos I, Rizzello L, Scurr DJ, Pompa PP, Bayer IS, Athanassiou A (2014) All-natural composite wound dressing films of essential oils encapsulated in sodium alginate with antimicrobial properties. Int J Pharm 463:137–145
23. Fatima H, Lee DW, Yun HJ, Kim KS (2018) Shape-controlled synthesis of magnetic Fe3O4 nanoparticles with different iron precursors and capping agents. RSC Adv 8:22917–22923
24. Buyana B, Aderibigbe BA, Ndinteh DT, Fonkui YT, Kumar P (2020) Alginate-pluronic topical gels loaded with thymol, norfloxacin and ZnO nanoparticles as potential wound dressings. J Drug Deliv Sci Technol 60:101960
25. Metwally F (2013) Evaluation of topical gel bases formulated with various essential oils for antibacterial activity against methicillin-resistant staphylococcus aureus. Trop J Pharm Res 12:877–884
26. Choudhary M, Chhabra P, Tyagi A, Singh H (2021) Scar free healing of full thickness diabetic wounds: a unique combination of silver nanoparticles as antimicrobial agent, calcium alginate nanoparticles as hemostatic agent, fresh blood as nutrient/growth factor supplier and chitosan as base matrix. Int J Biol Macromol 178:41–52
27. Khan AW, Kotta S, Ansari SH, Sharma RK, Kumar A, Ali J (2013) Formulation development, optimization and evaluation of aloe vera gel for wound healing. Pharmacogn Mag 9:S6-10
28. Siang R, Teo SY, Lee SY, Basavaraj AK, Koh RY, Rathbone MJ (2014) Formulation and evaluation of topical pentoxifylline-hydroxypropyl methylcellulose gels for wound healing application. Int J Pharm Pharm Sci 6:535–539
29. Rasul NH, Asdagh A, Pirsa S, Ghazanfarirad N, Sani IK (2022) Development of antimicrobial/antioxidant nanocomposite film based on fish skin gelatin and chickpea protein isolated containing Microencapsulated Nigella sativa essential oil and copper sulfide nanoparticles for extending minced meat shelf life. Mater Res Express 9:1–15
30. Fonkui TY, Ikhile MI, Muganza M, Fotsing MCD, Arderne C, Siwe-Noundou X, Krause RWM, Ndinteh DT, Njobeh PB (2018) Synthesis, characterization and biological applications of novel schiff bases of 2-(Trifluoromethoxy)aniline. J Chin Pharm Sci 27:307–323

31. Catanzano O, D'Esposito V, Formisano P, Boateng JS, Quaglia F (2018) Composite alginate-hyaluronan sponges for the delivery of tranexamic acid in postextractive alveolar wounds. J Pharm Sci 107:654–661
32. Patel S, Gheewala N, Suthar A, Shah A (2009) In-vitro cytotoxicity activity of solanum nigrum extract against Hela cell line and Vero cell line. Int J Pharm Sci 1:38–46
33. Felice F, Zambito Y, Belardinelli E, Fabiano A, Santoni T, Stefano RD (2015) Effect of different chitosan derivatives on in vitro scratch wound assay: a comparative study. Int J Biol Macromol 76:236–241
34. Suarez-arnedo A, Figueroa FT, Clavijo C, Arbela P, Cruz JC, Munoz-Camargo C (2020) An image J plugin for the high throughput image analysis of in vitro scratch wound healing assays. PLoS ONE 15:e0232565
35. Cheng Y, Hu Z, Zhao Y, Zou Z, Lu S, Zhang B, Li S (2019) Sponges of carboxymethyl chitosan grafted with collagen peptides for wound healing. Int J Mol Sci 20:3890
36. Ranzato E, Patrone M, Mazzucco L, Burlando B (2008) Platelet lysate stimulates wound repair of HaCaT keratinocytes. Br J Dermatol 159:537–545
37. Ramya Devi D, Sowmiya Lakshna S, Veena Parvathi S, Vedha Hari BN (2018) Investigation of wound healing effect of topical gel of Albizia amara leaves extract. South African J Bot 119:400–409
38. Balasubramanian K, Kodam KM (2014) Encapsulation of therapeutic lavender oil in an electrolyte assisted polyacrylonitrile nanofibres for antibacterial applications. RSC Adv 4:54892–54901
39. Sofi HS, Akram T, Tamboli AH, Majeed A, Shabir N, Sheikh FA (2019) Novel lavender oil and silver nanoparticles simultaneously loaded onto polyurethane nanofibers for wound-healing applications. Int J Pharm 569
40. Mahmood H, Khan IU, Asif M, Khan RU, Asghar S, Khalid I, Khalid SH, Irfan M, Rehman F, Shahzad Y, Yousaf AM, Younus A, Niazi ZR, Asim M (2021) In vitro and in vivo evaluation of gellan gum hydrogel films: assessing the co impact of therapeutic oils and ofloxacin on wound healing. Int J Biol Macromol 166:483–495
41. García C, Montero G, Coronado MA, Valdez B, Stoytcheva M, Rosas N, Torres R, Sagaste CA (2017) Valorization of eucalyptus leaves by essential oil extraction as an added value product in Mexico. Waste and Biomass Valor 8:1187–1197
42. Wang H, Liu Y, Cai K, Zhang B, Tang S, Zhang W, Liu W (2021) Antibacterial polysaccharide-based hydrogel dressing containing plant essential oil for burn wound healing. Burn Trauma 9:1–14
43. Boughendjioua H (2017) Fourier transformed infrared spectroscopy analysis of constituents of lemon essential oils from algeria. Am J Opt Photonics 5:30
44. Rezanejad R, Ojagh SM, Heidarieh M, Raeisi M, Rafiee G, Alishahi A (2019) Characterization of gamma-irradiated rosmarinus officinalis l. (rosemary). Turkish J Pharm Sci 16:43–47
45. Agatonovic-Kustrin S, Ristivojevic P, Gegechkori V, Litvinova TM, Morton DW (2020) Essential oil quality and purity evaluation via ft-ir spectroscopy and pattern recognition techniques. Appl Sci 10:1–12
46. Agnieszka N, Danuta K, Malgorzata P, Agata C (2013) Effects of thyme (Thymus vulgaris L.) and rosemary (Rosmarinus officinalis L.) essential oils on growth of Brochothrix thermosphacta. African J Microbiol Res 7:3396–3404
47. de Fernandes RV, B, Borges SV, Botrel DA, Oliveira CR de, (2014) Physical and chemical properties of encapsulated rosemary essential oil by spray drying using whey protein-inulin blends as carriers. Int J Food Sci Technol 49:1522–1529
48. Pirsa S, Asadzadeh F, Karimi Sani I (2020) Synthesis of magnetic gluten/pectin/Fe_3O_4 nano-hydrogel and its use to reduce environmental pollutants from lake urmia sediments. J Inorg Organomet Polym Mater 30:3188–3198
49. Kulkarni SA, Sawadh PS, Palei PK, Kokate KK (2014) Effect of synthesis route on the structural, optical and magnetic properties of Fe_3O_4 nanoparticles. Ceram Int 40:1945–1949
50. Awwad AM, Salem NM (2012) A green and facile approach for synthesis of magnetite nanoparticles. J Nanosci Nanotechnol 2:208–213
51. Hariani PL, Faizal M, Setiabudidaya D (2013) Synthesis and properties of Fe_3O_4 nanoparticles by co-precipitation method to removal procion dye. Int J Environ Sci Dev 4:336–340
52. Qureshi AA, Javed S, Javed HMA, Jamshaid M, Ali U, Akram MA (2022) Systematic investigation of structural, morphological, thermal, optoelectronic, and magnetic properties of high-purity hematite/magnetite nanoparticles for optoelectronics. Nanomaterials 12:1635

53. Lin YH, Lin JH, Hong YS (2017) Development of chitosan/poly-γ-glutamic acid/pluronic/curcumin nanoparticles in chitosan dressings for wound regeneration. J Biomed Mater Res B Appl Biomater 105:81–90
54. Li Y, Wang J, Yang Y, Shi J, Zhang H, Yao X, Chen W, Zhang X (2021) A rose bengal/graphene oxide/PVA hybrid hydrogel with enhanced mechanical properties and light-triggered antibacterial activity for wound treatment. Mater Sci Eng C 118:111447
55. Augustine R, Rehman SRU, Ahmed R, Zahid AA, Sharifi M, Falahati M, Hasan A (2020) Electrospun chitosan membranes containing bioactive and therapeutic agents for enhanced wound healing. Int J Biol Macromol 156:153–170
56. Ngece K, Aderibigbe BA, Ndinteh DT, Fonkui YT, Kumar P (2021) Alginate-gum acacia based sponges as potential wound dressings for exuding and bleeding wounds. Int J Biol Macromol 172:350–359
57. Ambekar RS, Kandasubramanian B (2019) Advancements in nanofibers for wound dressing: a review. Eur Polym J 117:304–336
58. Ahmad NS, Abdullah N, Yasin FM (2020) Toxicity assessment of reduced graphene oxide and titanium dioxide nanomaterials on gram-positive and gram-negative bacteria under normal laboratory lighting condition. Toxicol Rep 7:693–699
59. Huang X, Fu Q, Deng Y, Wang F, Xia B, Chen Z, Chen G (2021) Surface roughness of silk fibroin/alginate microspheres for rapid hemostasis in vitro and in vivo. Carbohydr Polym 253:117256
60. Standard I (2009) International Standard
61. Mukherjee D, Azamthulla M, Santhosh S, Dath G, Ghosh A, Natholia R, Anbu J, Teja BV, Muzammil KM (2018) Development and characterization of chitosan-based hydrogels as wound dressing materials. J Drug Deliv Sci Technol 46:498–510
62. Elmowafy M, Al-Sanea MM (2021) Nanostructured lipid carriers (NLCs) as drug delivery platform: advances in formulation and delivery strategies. Saudi Pharm J 29:999–1012
63. Mori HM, Kawanami H, Kawahata H, Aoki M (2016) Wound healing potential of lavender oil by acceleration of granulation and wound contraction through induction of TGF-β in a rat model. BMC Complement Altern Med 16:1–11
64. Pratama AM, Palinrungi AL (2022) An influence of topical treatment lavender essential oil on wound healing process through enhanced collagen synthesis and anti-microbial effects: a literature review. Int J Med Sci Clin Res Studies 2:1321–1324
65. Kazemi M, Mohammadifar M, Aghadavoud E, Vakili Z, Aarabi MH, Talaei SA (2020) Deep skin wound healing potential of lavender essential oil and licorice extract in a nanoemulsion form: biochemical, histopathological and gene expression evidences. J Tissue Viability 29:116–124
66. Kozics K, Bucková M, Puškárová A, Kalászová V, Cabicarová T, Pangallo D (2019) The effect of ten essential oils on several cutaneous drug-resistant microorganisms and their cyto/genotoxic and antioxidant properties. Molecules 24:1–15
67. Prashar A, Locke IC, Evans CS (2004) Cytotoxicity of lavender oil and its major components to human skin cells. Cell Prolif 37:221–229
68. Miastkowska M, Kantyka T, Bielecka E, Kałucka U, Kamińska M, Kucharska M, Kilanowicz A, Cudzik D, Cudzik K (2021) Enhanced biological activity of a novel preparation of lavandula angustifolia essential oil. Molecules 26:1–21
69. Ali M, Hassan A, Shah S, Rashid A, Naguib A (2022) The effect of tranexamic acid on the outcome of total ankle replacement. Cureus. https://doi.org/10.7759/cureus.26706
70. Ghaseminezhad SM, Shojaosadati SA, Meyer RL (2018) Ag/Fe3O4 nanocomposites penetrate and eradicate S. aureus biofilm in an in vitro chronic wound model. Coll Surf B 163:192–200
71. Moniri M, Moghaddam AB, Azizi S, Rahim RA, Saad WZ, Navaderi M, Arulselvan P, Mohamad R (2018) Molecular study of wound healing after using biosynthesized BNC/Fe3O4 nanocomposites assisted with a bioinformatics approach. Int J Nanomed 13:2955–2971

Publisher's Note Springer Nature remains neutral with regard to jurisdictional claims in published maps and institutional affiliations.